MODELING OF BO 105 FLIGHT DYNAMICS FOR RESEARCH ON FUEL SAVINGS DUE TO SINGLE-ENGINE OPERATION

M. Kerler, J. Hönle, H.-P. Kau
Institute for Flight Propulsion, Technische Universität München
Boltzmannstr. 15, 85747 Garching, Germany
martin.kerler@tum.de

Abstract

Performing a temporary shutdown of one engine of a twin-engine-powered helicopter in suitable situations during a flight mission saves fuel. Quantifying the potential fuel savings is a relevant item for both economic and environmental reasons. Before performing extensive and costly flight tests relevant simulations should be done. Therefore, in a first step, a cost-effective and detailed simulation model of the BO 105 for normal flight operations has been developed in MATLAB/Simulink, as part of a diploma thesis. The purpose was not to research new helicopter simulation methods but to select appropriate and approved methods to ensure a proper state-of-the-art simulation model. Besides the flight dynamics model, it includes a simple flight control system and an autopilot as well as a flight mission management system. In conjunction with the existing Allison 250-C20B simulation model of the Institute for Flight Propulsion, self-composed flight missions can be performed. The comprehensive model was validated with flight test data from the DLR, thereby demonstrating its prospects.

NOMENCLATURE AND ABBREVIATIONS

c	airfoil chord length
m	helicopter gross mass
$k_{(\dots)}$	controller gain values
p, q, r	roll, pitch, yaw rate (CGF)
$r, \Delta r$	rotor radius, radius increment
u_i	induced flow velocity
u_0	uniform induced flow velocity
u_c, u_s	longitudinal, lateral induced flow velocity
u_T, u_R, u_P	tangential, radial, parallel blade velocity
u, v, w	velocities (CGF)
x, y, z	distances
C_L, C_M, C_N	roll, pitch, yaw damping coefficient
C_L, C_D, C_Z	lift, drag, body drag coefficient
C_Z	vertical damping coefficient
$D, \Delta D$	drag, drag increment
F_x, F_y, F_z	blade-element forces
$[I]$	inertia tensor
$I_{xx}, I_{yy}, I_{zz}, I_{xz}, I_{zx}$	products of inertia
K_L, K_M, K_z	roll, pitch, vertical stiffness coefficient
K_N	yaw damping coefficient
$L, \Delta L$	lift, lift increment
$[L]$	inflow gain matrix
L, M, N	moments (CGF)
$[M]$	apparent mass matrix
N_b	number of rotor blades
N_r, N_ψ	number of radial, circumferential elements
Q	torque
R_i, R_o	inner, outer rotor radius
S	wake spacing state
T	thrust
U, U_∞	air velocities
$[V]$	mass flow parameter matrix
X	wake skew state
X, Y, Z	forces (CGF)
α	angle of attack
β	blade flapping angle, side slip angle
θ_0	collective pitch angle
θ_c, θ_s	longitudinal, lateral pitch angle
θ_{tw}	linear blade twist angle
κ_c, κ_s	lateral and longitudinal wake curvatures
λ_0	non-dimensional uniform inflow
λ_c, λ_s	longitudinal and lateral non-dimensional inflow
ρ	density
$[\tau_D]$	time constant matrix associated with wake distortion matrix
ψ	rotor azimuth angle
Φ, Θ, Ψ	roll, pitch, yaw angle
ϕ	section inflow angle
χ, χ_{end}	wake skew angle
Ω	rotor angular velocity
$(\dots)^*$	differentiate with respect to non-dimensional time

$(\ldots)_{qs}$	quasi-steady values
$(\ldots)_0$	values at rest
$(\ldots)_{is}$	actual values
$(\ldots)_{req}$	required/demanded values

BET	Blade Element Theory
DLR	Deutsches Zentrum für Luft- und Raumfahrt
ECEF	Earth Centered Earth Fixed Frame
FCS	Flight Control System
GB	Gearbox
GR	Ground
HTF	Horizontal Tail Frame
ISA	International Standard Atmosphere
Ma	Mach
MCS	Mission Control System
MR	Main Rotor
MRNF	Main Rotor Normal Frame
NED	North East Down
N1	Gas Generator Spool Speed
N2	Power Turbine Spool Speed
OEI	One Engine Inoperative
Re	Reynolds
SCMCS	Simulation Control and Mission Control System
TOW	Take Off Weight
TPP	Tip Path Plane
TR	Tail Rotor
TRNF	Tail Rotor Normal Frame
VTF	Vertical Tail Frame
WA	Wind Axis frame

1. INTRODUCTION

Most of the light and medium-class helicopters, like the Eurocopter EC135 and the Bell 412, are twin-engine-powered helicopters. This helicopter design is primarily driven by safety reasons. If an engine failure occurs, the remaining engine provides sufficient power to perform a controlled emergency landing. On the other hand, if both engines are fully functional they are operating with a partial load over a wide flight speed range since only a part of the available power is required for level flight. This can be seen in figure 1. The blue, green and orange curves represent the power required over flight speed for level flight at given helicopter gross masses at sea level. The red continuous line illustrates the available maximum continuous power of one engine; the red dashed line shows the total available maximum continuous power of two engines.

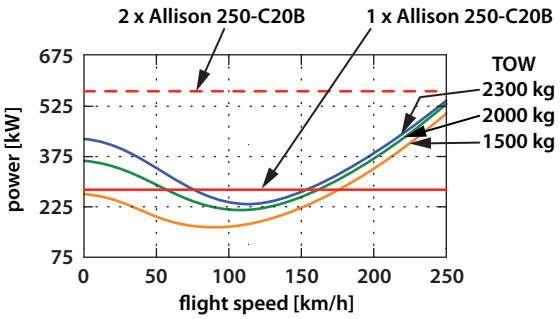

Figure 1: Power required over flight speed for different BO 105 gross masses [1]

As the specific fuel consumption decreases with increasing engine load, fuel can be saved by shutting down one engine and increasing the load of the remaining running engine. If this procedure is realized in the future, one constraint – in case of emergency – could be the ability to maintain a quick startup of the engine that has been shut down. Another constraint concerning this realization is its economic feasibility and thus the possibility of saving fuel.

Since the savings depend on the flight mission and on the period when one engine is inoperative, the fuel saving potential has to be determined. To get a first clue about the saving potential, simulations should be performed in advance.

The main requirements given to develop a suitable tool for such simulations are listed below:

- realization with MATLAB/Simulink
- simulation of the BO 105 flight dynamics
- possibility of integrating different engine models
- perform self-composed flight missions
- capability to run in real time including visualization

Also considering financial criteria and accessibility to commercial helicopter simulation tools, an existing tool could not be identified. Consequently, a tool for helicopter mission simulation, with a focus on the engine interface and the interchangeability of different engines, was developed at the Institute within six months, as a diploma thesis. Due to this time limit, current helicopter simulation aspects could merely be identified; the most suitable ones were used for the state-of-the-art helicopter simulation tool.

To meet all of the requirements, a non-linear flight dynamics model and a component-based modeling approach were chosen. This enables an unproblematic replacement of the simulation model components, which is required if more detailed components are to be integrated easily. Hence, in

the event that simulating a helicopter type other than the BO 105 is simulated, the non-linear flight dynamics model can be adopted with little modeling effort. In addition, the flight dynamics model is able to cover the whole flight envelope and the helicopters' motion can be computed in real time [2]. Overall, this results in the Simulink model whose top level is shown simplified schematically in figure 2.

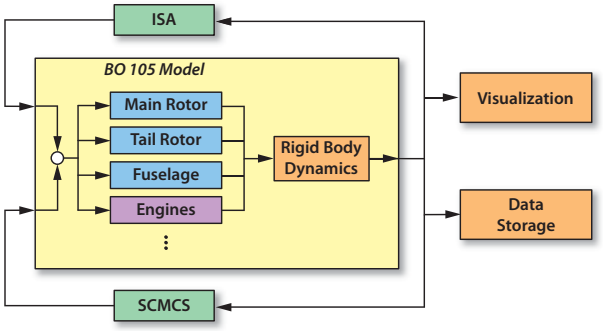

Figure 2: Top level of the implemented Simulink model

The main modules of the BO 105 helicopter model and the flight dynamics modeling approach are described in section 2. The overall helicopter module is divided into several sub-components that represent, for instance, the main rotor, tail rotor or fuselage. After that, a short overview is given of the combination of the flight control system (FCS) and the autopilot. Another relevant part of the simulation model is the Simulation Control and Mission Control System (SCMCS) component in section 4. The modeling concludes with the model validation based on flight test data.

2. BO 105 FLIGHT DYNAMICS MODELING

To cover the whole flight envelope [2], a non-linear flight dynamics model has been developed. The model is divided into several sub-components, e.g. the main rotor component, the tail rotor component and the fuselage component. Each of these component models describes its related physical properties. The main deliverables are forces and moments with respect to the helicopter's center of gravity. The helicopter itself is treated as a rigid body and has a defined center of gravity. The forces and moments of the components are input from the rigid body dynamics component. This calculates the motion of the rigid body through space and the body's attitude within a total of six degrees of freedom. Therefore, the differential equations of motion are used. For the accelerations in the body fixed frame:

$$(1) \qquad \begin{bmatrix} X \\ Y \\ Z \end{bmatrix} = m \cdot \left(\begin{bmatrix} \dot{u} \\ \dot{v} \\ \dot{w} \end{bmatrix} + \begin{bmatrix} p \\ q \\ r \end{bmatrix} \times \begin{bmatrix} u \\ v \\ w \end{bmatrix} \right)$$

The angular acceleration in the body fixed frame can be calculated as follows:

$$(2) \qquad \begin{bmatrix} L \\ M \\ N \end{bmatrix} = [I] \cdot \begin{bmatrix} \dot{p} \\ \dot{q} \\ \dot{r} \end{bmatrix} + \begin{bmatrix} p \\ q \\ r \end{bmatrix} \times \left([I] \cdot \begin{bmatrix} p \\ q \\ r \end{bmatrix} \right)$$

The inertia tensor $[I]$ is defined as follows:

$$(3) \qquad [I] = \begin{bmatrix} I_{xx} & 0 & I_{xz} \\ 0 & I_{yy} & 0 \\ I_{zx} & 0 & I_{zz} \end{bmatrix}$$

As the helicopter is almost axis-symmetrical, the values of I_{xy} and I_{yx} are neglected and thus set to zero. The inertia tensor stays constant over the mission time despite the change in remaining fuel mass within the helicopter. X, Y and Z are forces defined in the body-fixed frame. L, M and N are values of the moment vector and are defined in the body-fixed frame. The body-fixed frame in this simulation model is called the Center of Gravity Frame (CGF). The main frames used in this simulation are illustrated in figure 3.

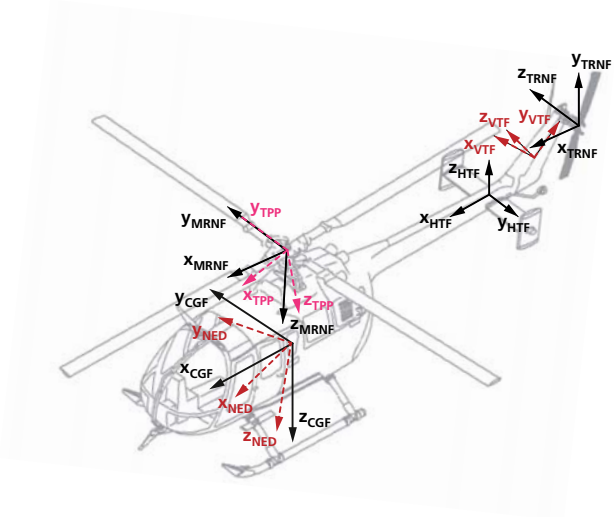

Figure 3: Main frames of the simulation model

Due to different mission requirements (e.g. people rescue, water drop) and because of fuel consumption over mission time, the helicopter's mass can be variable.

The description of the helicopter's orientation in space is realized by Euler angles. These angles define the attitude of the CGF with respect to the North East Down (NED) frame. The Euler angle's rate of change has a relationship to the body-fixed angular velocity vector $(p, q, r)^{-1}$.

$$(4) \qquad \begin{bmatrix} \dot{\Phi} \\ \dot{\Theta} \\ \dot{\Psi} \end{bmatrix} = \begin{bmatrix} 1 & \sin\Phi\cos\Theta & \cos\Phi\tan\Theta \\ 0 & \cos\Phi & -\sin\Phi \\ 0 & \sin\Phi\sec\Theta & \cos\Phi\sec\Theta \end{bmatrix} \begin{bmatrix} p \\ q \\ r \end{bmatrix}$$

A disadvantage of this transformation is the possibility of singularities, depending on the angles. To avoid the so-called Gimbal Lock [18], Quaterions are used to compute the orientation in space.

2.1. Main rotor model

A common approach in helicopter dynamics modeling was used to calculate the forces and moments of the main and tail rotor. It consists of three main parts: dynamic inflow model, blade element forces and blade dynamics.

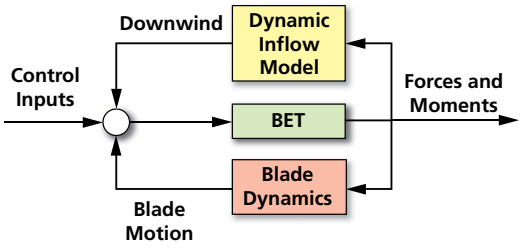

Figure 4: Scheme of the rotor model [3]

The dynamic inflow model is used to determine the inflow distribution of the rotor. Earlier helicopter simulations implemented a uniform inflow distribution. This approach is applicable for hovering flight states but not utile for forward flight states, for instance. Pitt and Peters [4] developed a dynamic inflow model with three inflow states λ_0, λ_s and λ_c. It is valid for hover and forward flight. By implementing some adoptions it can also be used for sideward flight. The states are related to the thrust coefficient C_T and the rolling and pitching coefficients C_M and C_L by a first-order differential equation system:

$$(5) \qquad [M]\begin{bmatrix}\dot{\lambda_0}\\ \dot{\lambda_s}\\ \dot{\lambda_c}\end{bmatrix} + [L]^{-1}[V]\begin{bmatrix}\lambda_0\\ \lambda_s\\ \lambda_c\end{bmatrix} = \begin{bmatrix}C_T\\ -C_L\\ -C_M\end{bmatrix}_{wa}$$

$[M]$ is the apparent mass matrix, $[V]$ represents the mass flow parameter matrix and $[L]$ is the inflow gain matrix. A detailed description of the dynamic inflow model can be found in [4]. In this simulation model, the implemented dynamic inflow model was extended for predicting an off-axis response. For this purpose, Zhao's approach [5] is implemented, which describes the distortion of the wake geometry during flight maneuvers. Three disturbances were detected: gradual changes in wake bending (lateral and longitudinal), wake skew and wake spacing. The resulting effect is represented by a set of first-order differential equations [5][6].

$$(6) \qquad [\tau_D]\begin{bmatrix}X\\ S\\ \kappa_c\\ \kappa_s\end{bmatrix}^{*} + \begin{bmatrix}X\\ S\\ \kappa_c\\ \kappa_s\end{bmatrix} = \begin{bmatrix}X\\ S\\ \kappa_c\\ \kappa_s\end{bmatrix}_{qs}$$

In general, the matrix containing the non-dimensional time constants $[\tau_D]$ is fully populated. However, the interaction between the four states is neglected, which leads to a diagonal form. The abbreviation *qs* stands for quasi-steady values. These values are used to calculate the resulting wake skew angle χ_{end} as the sum of the steady wake skew angle χ and the quasi-steady one.

$$(7) \qquad \chi_{end} = \chi + \chi_{qs}$$

The wake skew angle is relevant for flow interactions at the horizontal and vertical tail. Furthermore, the original inflow gain matrix $[L]$ by Pitt and Peters [4] is manipulated by three additional matrices, which represent different links between the wake skew curvature, the wake skew angle and the rotor loadings. In summary, the inflow distribution and the wake skew angle can be calculated.

These values provide indispensable input for the blade element theory. A single blade is divided into very small blade segments, each representing an airfoil cross-section. With known C_L and C_D values of the airfoil, the lift and drag forces at the blade element can be determined with the formulas 8 and 9:

$$(8) \qquad \Delta L = \frac{1}{2}\cdot\rho\cdot U^2\cdot C_L\cdot c\cdot\Delta r$$

$$(9) \qquad \Delta D = \frac{1}{2}\cdot\rho\cdot U^2\cdot C_D\cdot c\cdot\Delta r$$

The lift and drag coefficients depend on the local Mach and Reynolds numbers. As the blade elements have inflow velocities from Mach 0 to almost Mach 1 at fast forward flight, a sophisticated data set of coefficients is necessary. Due to the lack of measurement data from wind tunnel tests, another approach was used to determine the coefficients between ranges from $Re = 2.5\cdot10^6$ to $Re = 6.5\cdot10^6$ and from $Ma = 0.0$ to $Ma = 0.8$. The computer program XFOIL was used to determine the coefficients C_L and C_D depending on the angle of attack, Mach and Reynolds numbers. As it is designed for subsonic airfoils and incompressible flow, the results were satisfactory for low Mach numbers. Above $Ma = 0.5$, the calculated values roused suspicion, and the lift and drag polars had to be extrapolated. For usage in a Simulink S-function, the polars were approximated by a polynomial function with a degree of 6. The resulting functions over the angle of attack can be seen in figure 5.

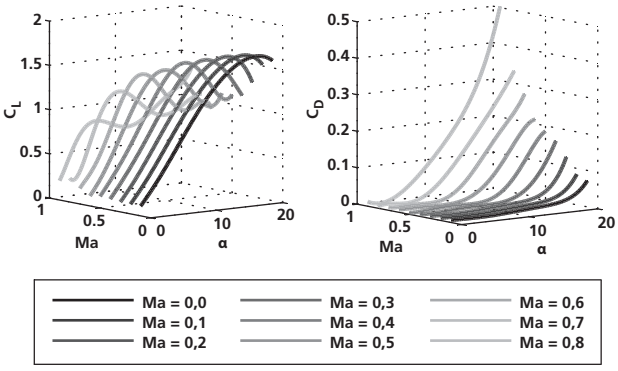

Figure 5: C_L and C_D over α for $Re = 3.5\cdot10^6$

The notation of Johnson [7] is used for determining the local air speeds at the blade segments. In this case, the pitch angle θ of the blade element is a function of the collective and cyclical pitch angles as well as the linear blade twist of the BO 105 main rotor blades.

(10) $\theta(r,\psi) = \theta_0 + \theta_c \cdot \cos\psi + \theta_s \cdot \sin\psi + r \cdot \theta_{tw}$

The difference between the blade element pitch angle and the section inflow angle ϕ is the relevant angle of attack for further lift and drag calculations. The required air speed U is based on the tangential and parallel air speeds at the blade element.

(11) $U = \sqrt{u_T^2 + u_R^2}$

(12) $u_T(r,\psi) = \Omega \cdot r + U_\infty \cdot \sin\psi$

(13) $u_R(r,\psi) = U_\infty \cdot \cos\psi$

As can be seen in equation 12, the tangential velocity component depends on the rotational speed Ω and the blade element radius r as well as the overall helicopter velocity transformed into the main rotor frame and depending on the blade elements peripheral angle. The velocity component u_P normal to the main rotor frame considers the flapping angle β of the rotor blade, the rate of flapping $\dot{\beta}$ and the velocity due to downwash u_i as well as the axial motion u_f. Pitt and Peters describe the inflow velocity at different rotor positions as follows.

(14) $u_i(r,\psi) = u_0 + u_c \cdot \frac{r}{R} \cdot \cos\psi + u_s \cdot \frac{r}{R} \cdot \sin\psi$

The inflow velocities $u_{(\dots)}$ are related to the inflow states via the correlation $u_{(\dots)} = \lambda_{(\dots)} \cdot \Omega \cdot R$. For blade flapping angle calculations, the equations derived from the equilibrium of hinge moments in [8] are used.

Finally, the forces at the blade element are defined.

(15) $dF_z = dL \cdot \cos\phi - dD \cdot \sin\phi$

(16) $dF_x = dL \cdot \sin\phi - dD \cdot \cos\phi$

(17) $dF_y = -\beta \cdot dF_z + D_{radial}$

The drag in radial direction will be neglected due to its small value compared to the other forces. For determining the main rotor's overall forces, the forces of the blade elements have to be integrated over radius and circumference and then multiplied by the number of blades. Equation 18 shows this for the main rotor thrust.

(18) $T = \frac{N_b}{2\pi} \int_0^{2\pi} \int_0^R F_z dr d\psi$

As the functions become too complex to be integrated, an approximation is done using sums. Therefore, the rotor area has been divided in the radial direction into 20 segments of equal length. In the circumferential direction, 75 segments were chosen after analyzing calculation accuracy. Overall, forces are evaluated at 1,500 points on the rotor area.

(19) $T = \frac{N_b}{2\pi} \sum_1^{N_\psi} \sum_1^{N_r} F_z \Delta r \Delta\psi$

(20) $\Delta r = \frac{R_o - R_i}{N_r}$

(21) $\Delta\psi = \frac{2\pi}{N_\psi}$

The summation and the overall computation of the main rotor forces and moments is realized with a Simulink S-function written in C-code.

As the two for-loops of the S-function influence the computation time, an investigation was done regarding the computation performance. Two simulations of 50 and 80 seconds were designed to test the performance of the code on three different computers. One of these is a personal notebook (computer 3) and two are desktop computers (computer 1 and 2). Furthermore, three different discretizations were tested. The first one divides the rotor blade radially into 5 elements and circumferentially into 25 elements (125 elements in total). The second one splits the blades radially into 10 and circumferentially into 50 pieces (500 elements in total). The last one has 20 in the radial and 75 in the circumferential direction (1500 elements in total). The computation time results for the 80 seconds simulation are shown in table 1.

	5/25	***10/50***	***20/75***
Computer 1 (2x1.86 Ghz)	1.853 s	3.826 s	9.520 s
Computer 2 (6x3.00 Ghz)	0.769 s	1.535 s	3.718 s
Computer 3 (2x2.00 Ghz)	1.445 s	3.166 s	7.918 s

Table 1: CPU times used for different discretizations

It can be seen that the hexa-core CPU with the highest clock rate is more than twice as fast as the second-fastest one. Furthermore, it takes approximately a tenth of the simulation time to compute the most accurate discretization available.

Another investigation regarding different rotor area discretization was the accuracy of the calculated forces and moments. In particular, the torque of the main rotor shaft is directly related to the power. Thus, several simulations of the main rotor component were performed. One is the increase and decrease of the collective pitch, as can be seen in figure 6 a). Figure 6 b) plots the equivalent main rotor torque. The most accurate discretization was set as a reference. Figures 6 c) and d) show the relative divergence of the 10/50 and 5/25 discretization.

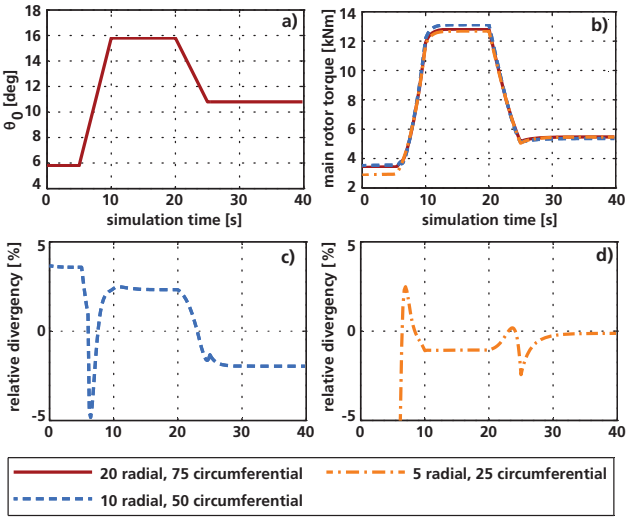

Figure 6: Comparing the divergence for different discretization

In this special case, the 5/25 discretization sometimes shows a better characteristic than the 10/50 discretization in comparison to the 20/75 discretization. Further simulations with other boundary conditions showed a similar behavior. In conclusion, the 20/75 discretization was taken to provide a sufficient accuracy.

To reduce complexity and effort, some simplifications were made. The lead-lag motion of the blades is set to zero. Only the flap motion is considered. Furthermore, the blades are assumed to be rigid. Thus, blade bending does not have any influence on the dynamic behavior in this simulation. Several aerodynamic effects are also neglected, for example the dynamic stall and the reverse flow effect at high flight speeds. Also tip losses at the blades were not considered before the model was slightly corrected.

2.2. Tail rotor model

The power required for the tail rotor is nine to ten times lower than the power required for the main rotor, as stated in [9]. Thus, the model accuracy is not as high as the one for the main rotor, though similar model components are used. Simplifications are made by reducing the complexity of the components. For example, the flapping angles are neglected; and due to the helicopter's control mechanisms, blade angle is only controlled by collective pitch.

In comparison to the main rotor, the angles of attack at the tail rotor blades are within a wider range than the ones of the main rotor, due to sideward flight, yaw motion or main rotor downwash. Thus, a different approach is used to determine the α dependent C_L and C_D values of the NACA 0012 airfoil used. In [10], these values were gathered for the angles of attack from $0°$ up to $180°$. The company Cyberiad [11] utilized this data set to determine the values for useful Re numbers such as $Re = 2.0 \cdot 10^6$. The results for C_L and C_D can be seen in figure 6.

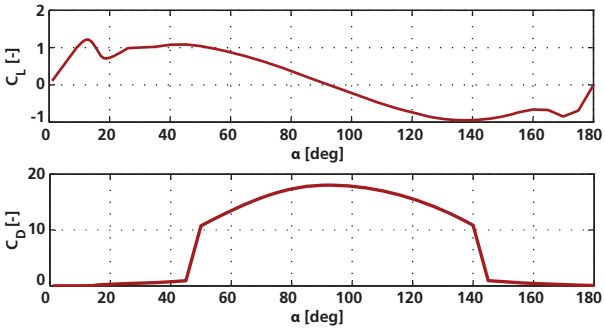

Figure 7: Used NACA 0012 airfoil polars [11]

The polars are split into several angle of attack regions in which the polars can be approximated by polynomial functions with a degree of 6.

2.3. Fuselage model

In terms of volume, the fuselage is one of the greatest components of the BO 105; due to drag at higher flight velocities, it has a significant influence on the flight performance. Therefore, it is necessary to determine the fuselage's lift and drag according to the flight velocity, angle of attack and side slip angle. According to [12], wind tunnel measurements containing the BO 105 fuselage were taken. The angles for side slip and attack range from $-15°$ to $+15°$. As greater ranges are required the measured lift and drag polars have to be extended. For an UH-60 helicopter, polars are available in [13] for an angle range from $-90°$ up to $+90°$. On this basis the BO 105 polars were modified to match the UH-60 polars, not quantitatively but qualitatively in angle ranges where no BO 105 wind tunnel data was available. For usage in the simulation, the polars are approximated by functions of the angle of attack and side slip angle. An example of a function is given for the fuselage lift in equation 22.

(22) $$C_Z = (1 - |\sin\beta|) \cdot (17 \cdot \sin^2\alpha - 2)$$

The overall lift and drag polars are pictured in figure 8.

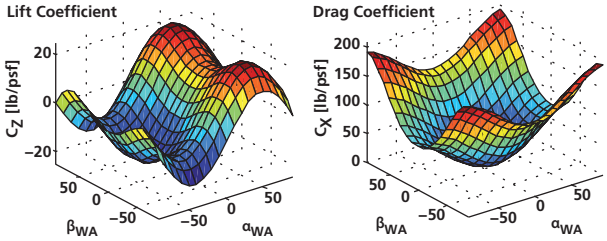

Figure 8: Lift and drag coefficients for different α and β in the wind axis frame

The coefficients for lift, drag and pitch moment are functions of the angle of attack and the side slip angle. The coefficients for side force, roll moment and yaw moment depend only on the side slip angle in this simulation model.

One limitation of the fuselage drag model is its validity only for angles ranging from $-90°$ to $+90°$. No coefficient data was available for backward flight, for instance. Thus, for backward flight, the equivalent values as for forward flight are used.

2.4. Empennage model

Another two components that have an influence on the helicopter dynamics are the horizontal and the vertical stabilizer. The air flow around these two planes is very complex due to the main and tail rotor downwash as well as turbulence caused by the fuselage. So its models have to be simplified.

In figure 9 the influence of the main rotor downwash on the horizontal and vertical stabilizer can be seen in a simplified way.

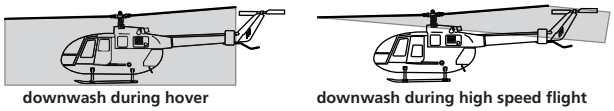

Figure 9: Influence of the downwash on the horizontal and vertical stabilizer

If there is no reduction of the main rotor wake tube diameter in the downstream direction, the horizontal stabilizer is mostly inside this wake tube. If the wake angle χ is greater than about $85°$ at high-speed flights, the influence of the main rotor downwash on the horizontal stabilizer vanishes. Between these two flight states, the percentage of influence is modeled by a simple linear function. Nevertheless, the horizontal tail has inflow angles from $0°$ up to $360°$. As the symmetrical NACA 0012 airfoil is used, the requirements for lift and drag polars are reduced for a data set from $0°$ up to $180°$. The polars are already known from the tail rotor blades.

Even the downwash of the tail rotor is neglected at the horizontal stabilizer. It is only taken into account by the vertical stabilizer. Thus, using simple functions, the percentage of the influence of the main and as well as tail rotor downwash is identified depending on the flight state. This is used to define the velocity and the angle of attack at the vertical stabilizer. The vertical stabilizer has an unknown airfoil. Due to the lack of lift and drag coefficients, the known NACA 0012 airfoil is used instead.

2.5. Skid model

As one intention of the BO 105 flight dynamics model is to cover all flight states in a normal helicopter mission, the interactions between ground and helicopter have to be simulated. Beaulieu stated in [13] that there is very little literature about helicopter ground dynamics and especially modeling ground reaction forces of helicopter skids. Generally, two methods are applied in common simulations. One is the impulse method and the other is the penalty method, which is used by Johnson [15] for the simulation of a small unmanned helicopter. Due to the simpler implementation of the penalty method and the demonstration of its abilities, it has been chosen for the BO 105 flight dynamics.

The penalty method model defines the earth's surface as a spring damper system that pushes the helicopter back if its skid penetrates the ground. The BO 105 has a skid made up of steel tubes which would penetrate the ground along two parallel lines. Due to simplification of the calculation, the two lines are replaced by four contact points. One contact point is located at each end of the tubes. Thus, the positions of the contact points are known; depending on the helicopter's motion and attitude, each contact point has a certain position in space and a certain velocity. Using this data, the sub-component Contact Point Logic detects any contact with the ground. The sub-component Contact Point Velocity gives information about the penetration velocity in the three frame directions. The scheme of the entire Ground Reactions component can be seen in figure 10.

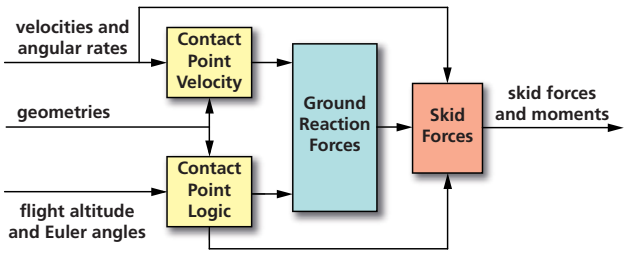

Figure 10: Scheme of the Ground Reactions component

Using the penetration depth Δz and velocity $\dot{z}$ of a contact point, the ground reaction forces in the vertical direction are calculated according to equation 23.

$$F_{z,react} = F_{z,heli} - C_z \cdot \dot{z} - K_z \cdot \Delta z \tag{23}$$

As there were no reasonable values available for the damping coefficients $C_{(\dots)}$ and the spring stiffness coefficients $K_{(\dots)}$, the values were determined empirically. In the horizontal direction the forces in the x and y direction can be interpreted as static and dynamic friction forces. First, using the static friction coefficient and the normal force at the contact point,

the static friction force is calculated. After that, the reaction forces of the spring damper system in the x and y direction are calculated. If these forces are less than the static friction forces, the helicopter remains in a stationary position and the forces of the skid acting on the helicopter's center of gravity are the spring damper system forces. In the other case, the resulting skid forces are calculated using the dynamic friction coefficient if the contact point motion is greater than $1\ m/s$ in the x-y plane.

Due to the skid force vector displacement from the center of gravity, the helicopter encounters moments, caused by the skid. These moments are mainly pitch and roll moments. Beaulieu [14] describes them as pivot and oscillation moments, as can be seen in figure 11.

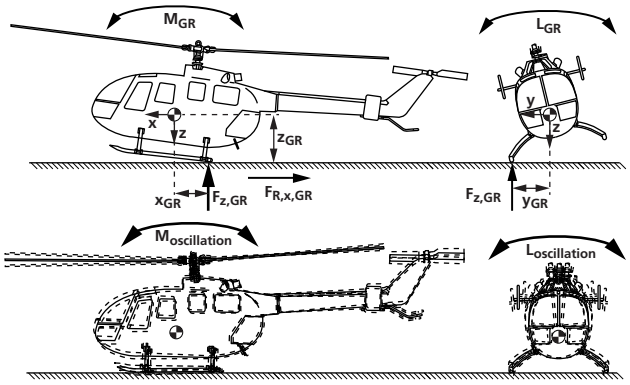

Figure 11: Pivot and oscillation moments

The governing equations are:

(24) $$L_{oscillation} = -K_L \cdot (\Phi - \Phi_0) - C_L \cdot (p - p_0)$$

(25) $$M_{oscillation} = -K_M \cdot (\Theta - \Theta_0) - C_M \cdot (q - q_0)$$

However, Beaulieu [14] stated, that the parameters K_L, K_M as well as C_L and C_M, are neither stiffness nor damping constants, but can be considered as a resistance to roll and pitch movements. Φ_0 and Θ_0 are values for the helicopter standing on the ground. Assuming a flat plane, these values are $\Phi_0 = 0°$ and $\Theta_0 = 1.5°$. Furthermore, if the helicopter is on the ground, p_0 and q_0 are zero.

Regarding the yaw motion during ground contact, a damping term is used.

(26) $$N_{damping} = -K_N \cdot (\Psi - \Psi_{req}) - C_N \cdot r$$

The difference of Ψ and Ψ_{req} is used to reduce the introduced reaction moment due to the yaw rate r. Overall, the simulation of the skid forces and moments showed good results. The skid model is valid for decent rates up to $2\ m/s$.

2.6. Power train / Engine model

In this simulation model, the entire power train consists of the engines, gearboxes and shafts. Figure 12 visualizes the linkage between these powertrain model sub-components.

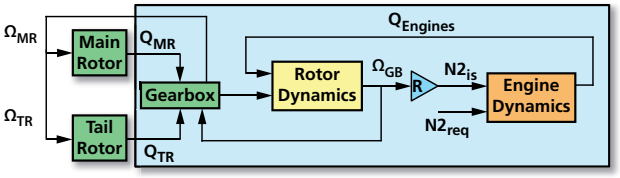

Figure 12: Scheme of the power train model

The general rotor dynamics of the power train are represented by equation 27.

(27) $$\dot{\Omega}_{GB} = \frac{Q_{Engines} - Q_{GB}}{J}$$

Where Q_{GB} is the torque required by both rotors and $Q_{Engines}$ is the torque provided by both engines. If the sum of these values differs from zero, the rotational speed changes with respect to the overall torque of inertia J. As the rotational speed of the rotor is to be kept constant, the engines have to provide sufficient power inside the flight envelope.

The Allison 250-C20B engine model is a state space model implemented in Simulink and was developed by the institute. Thus, it can be used here as a black box with well-defined inputs and outputs. These ports are environmental parameters, collective pitch, actual and required N2 rotational speed as well as the fuel flow and the provided torque of the power turbine. The engine model is valid within the range of 0% - 100% rotational speed of the N1 shaft. Thus, the whole engine operating range, including start and shutdown, can be simulated. Additionally, the engine model is validated for quick starts on the ground and during flight.

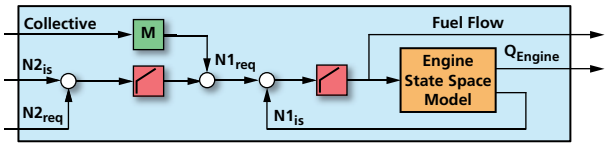

Figure 13: Simplified scheme of the engine control mechanism

For the engine control, PI controllers and look-up tables are used. The engine model has been validated with the recorded data at the engine test bed of the institute.

3. FLIGHT CONTROL SYSTEM (FCS)

Due to the requirement of autonomous mission accomplishment an adequate flight control system (FCS) is realized. The FCS is capable of performing helicopter starts, flight maneuvers and landings determined by certain values. For example, flight maneuvers include climbing and descending with

forward speed, accelerating and decelerating, hovering as well as vertical climbing and descending. The FCS covers all four control axes, and the command variables are provided by the Mission Control System (SCMCS). The main concept of the SCMCS is described in the next chapter.

Usually a pilot operates the helicopter by means of a stick, lever and pedals. His commands are transferred to the rotors via cables or rods. Often, interconnected actuators enforce the commands. Due to simplification, this transmission path is omitted, thus FCS commands are directly equivalent to blade pitch angles and provide straight inputs for the rotor models.

Further constraints for a FCS come from guaranteeing a certain level of flight comfort. In addition, excessive control inputs, which may lead to structural damage and flight instabilities, are avoided. At an early stage of FCS development, the model was not able to comply with these constraints. The problem was solved by reducing the step size between the command and state variables. To overcome the phase lag effect, a mixing unit for the cyclic pitch is integrated using a phase angle of $12°$.

Usually, there is a differentiation between the autopilot, the flight stability system and the flight control system. In most cases, the last two systems are combined into the Control and Stability Augmentation System to reduce the pilot's workload. The FCS developed for this simulation combines them into the overall FCS.

As the development of a sophisticated flight controller was not the focus of this project, simple PI controllers with state feedback are used for the four axis controls. The scheme of one can be seen in figure 14. The corresponding gains were empirically determined during the FCS development phase.

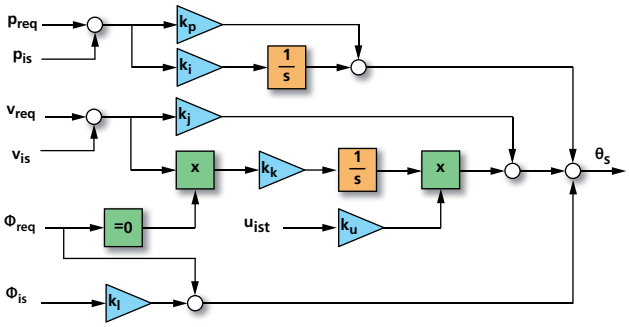

Figure 14: Scheme of controller for θ_s

The maximum values of the delivered blade command angles are given by real helicopter's mechanical limits. In addition the command angles' maximum change rate is set to $20°/s$.

4. SIMULATION CONTROL AND MISSION CONTROL SYSTEM (SCMCS)

The Simulation Control and Mission Control System (SCMCS) is in charge of managing the simulation itself and providing the command variables for the FCS. Simulation Control refers to initializing the simulation model, accomplishing of the actual flight mission and data post-processing after the end of the flight mission. During the initialization phase, the helicopter is a few centimeters above the ground surface. Then, it accelerates vertically due to gravity until the ground reaction forces are fully developed. Furthermore, all of the blade command angles are set to zero and both engines are shut down. After this short phase, the SCMCS switches into the mission control mode for accomplishing the mission.

The mission control mode governs the flight mission. Therefore, a Simulink Stateflow model is used to provide the adequate values for the FCS depending on the flight mission element. This includes, among other things, engine control signals and blade pitch commands. The flight mission itself consists of a table where every row defines a certain part of the mission. The distinguishing flight parameters are stored in the cells of a mission element. These parameters are mainly:

- length of the mission element if required
- parameters to select the required Stateflow box
- three flight velocity parameters
- pitch, yaw and roll rates
- three parameters for ECEF positioning
- required azimuth and roll angle

The observer of the Stateflow model processes the mission element table row by row and selects the related state depending on the flight mission. If the current mission element is finished or the desired flight states are reached, the observer selects the next row in the flight mission element table and chooses the related state. The principal scheme of the MCS can be seen in figure 15.

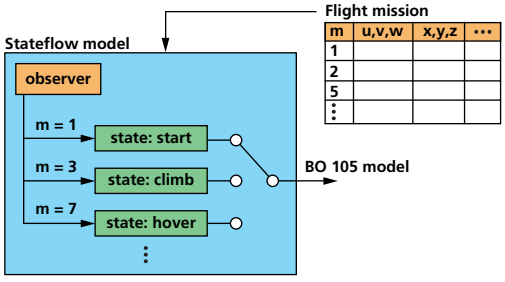

Figure 15: Scheme of the principal MCS function

An advantage of the SCMCS is the repeatability of missions. This is useful if the same mission will be operated partly with one engine inoperative (OEI). Hence, the results of the flights with and without OEI can be directly compared.

The Stateflow model defines the available mission elements; the flight missions can consist of multiple elements with different flight state values. Besides these advantages there are some drawbacks. Until now, no real 3D or 4D navigation has been implemented, and some mission elements are still constrained. For instance, forward flight can only be specified by time with a constant speed, azimuth and altitude.

In summary, the SCMCS provides enough functionality to accomplish the usual helicopter flight missions in a proper way.

5. VALIDATION

After model development is finished, the model has to be validated using flight test data. As the focus is not to precisely simulate the flight dynamics of the BO 105, the validation is done for the steady-state case. For this purpose, flight test data from Germany's national research center for aeronautics and space (DLR) were available. The flight test data provides, among other things, values for collective and cyclic pitch for certain flight speeds. The tests were performed by the DLR BO 105 S123 research helicopter at a flight altitude of 3300 ft and with a gross mass of 2200 kg. Several authors used the data as reference [16] [17]. The following chapter, describes some results of the validation.

A first comparison leads to the results shown in figure 16.

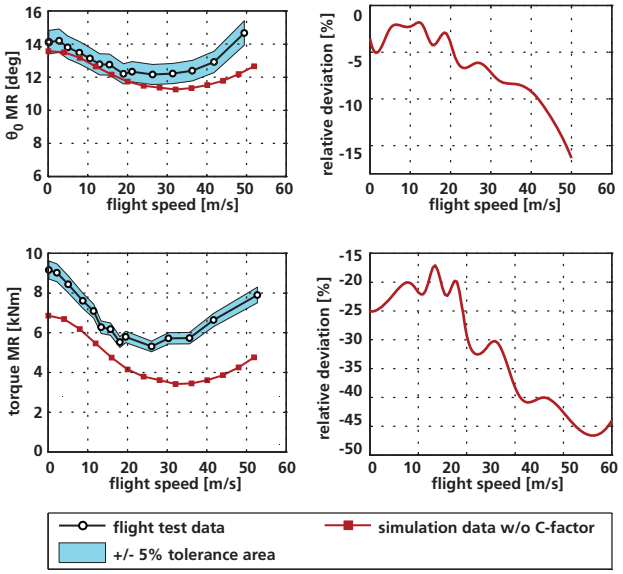

Figure 16: Collective pitch θ_0 and main rotor torque validation (without C-factors)

The left plot presents the results of the simulation and the flight test data. In addition, a tolerance area of $+5\%$ and -5% offset from the flight test data is marked. The plots on the right indicate the relative deviation of the simulation data to the flight test data.

The θ_0 polar matches flight test data for flight speeds below $20\,m/s$ well. For faster flight speeds, the data polars of the flight test and of the simulation start to diverge. One reason for such a behavior can be too-low drag coefficients for the fuselage and too-high lift coefficients for the rotor blades. An obvious mismatch can be seen in the torque polars. Although the polars are qualitatively similar, from a quantitative point of view the difference cannot be accepted. The huge deviation is valid for the whole flight speed range and is likely to be caused by too-low drag coefficients of the main rotor blades.

Finally, this first validation run gives hints about which parts of the simulation model have to be modified for better matching. As expected, due to the known shortfalls of XFOIL, the lift and drag coefficients were each modified with a correction factor (C-factor). The same was done for the drag coefficient C_X of the fuselage because it is unknown whether the drag of the main rotor hub has been considered in the wind tunnel measurements. Despite the accuracy deficiencies of the model, the flight test data shows a scattered characteristic around flight speeds of $15\,m/s$. Thus, matching the flight test data curve is rather difficult.

After updating the flight dynamic model with the three correction factors, the validation was performed again. The results are displayed in figure 17.

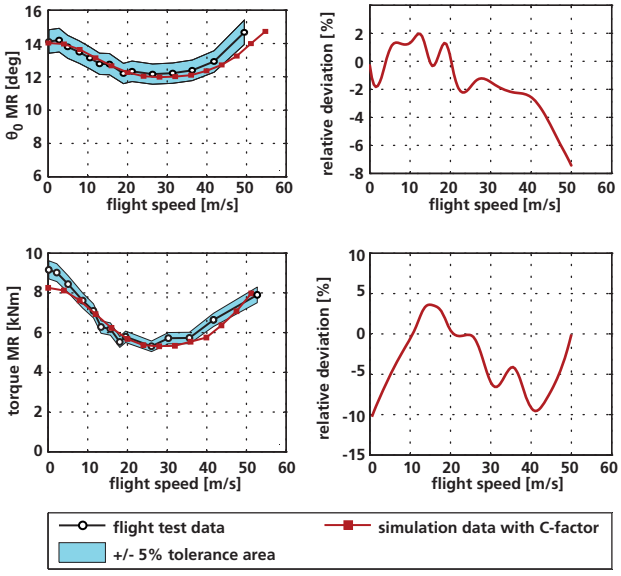

Figure 17: Collective pitch θ_0 and main rotor torque validation (with C-factors)

As one can see in the collective pitch diagram, the relative deviation decreases and the simulation

accuracy is satisfactory. The more relevant value for determining fuel consumption is the amount of power required, and thus the required torque. In comparison to the simulation model without correction factors, the simulation accuracy increased considerably. The main purpose was hitting the $\pm 5\%$ tolerance area, which was almost reached. At low flight speeds and at flight speeds around $40\,m/s$, there is a lack of sufficient accuracy. One reason for this could be the neglected drag of the fuselage due to the main rotor downwash, or aerodynamic effects that were not taken into account.

In summary, the accuracy of the simulation model was enhanced by using three correction factors. The remaining small deviations are acceptable in the light of the simplicity of the model.

6. CONCLUSION AND OUTLOOK

This paper gives an overview of the development of a helicopter mission simulation tool. Therefore, the principal design of the main components is described. The helicopter itself is modeled as a rigid body with six degrees of freedom and variable mass. Its drag and lift are estimated by coefficients depending on its attitude. For the main rotor, an extended dynamic inflow model is used. Forces and moments of blades and the empennage are generally computed using blade-element theory. The contact between skid and ground is assumed as a spring damper system for determining the ground reaction forces. A state space model of the Allison 250 C20B engine, which was developed at the Institute for Flight Propulsion, has been integrated into the overall simulation model. A simple flight control system has been implemented to control the helicopter in almost every area of the flight envelope. Additionally, a system has been realized for controlling the simulation itself and for performing the flight mission. Flight missions are split into mission elements, and each of these is stored in a table as a row. This table is then executed row by row. After the simulation model's implementation a validation with flight test data was performed and the helicopter dynamics model was slightly improved.

Now the Institute for Flight Propulsion is capable of performing different helicopter flight missions with and without shutting down one engine for fuel savings. Further research will concern the quantification of fuel saved during diverse flight missions. In addition, the flight dynamics model should be validated in its dynamic behavior, and the simulation model components can still be improved to achieve better simulation accuracy and thus more meaningful results.

7. ACKNOWLEDGEMENT

The authors would like to thank Dr. Grünhagen and Dr. Kessler from DLR for their support concerning flight test data for the BO 105 helicopter.

8. REFERENCES

[1] C. KESSLER: Leistungsbedarf und Steigleistung. In *Entwurfsgrundlagen der Drehflügler*, University lecture, Munich, 2007

[2] M. ROHLFS, W. V. GRÜNHAGEN, J. KALETKA: Nonlinear Rotorcraft Modeling and Identification. In *RTO SCI Symposium on 'System Identification for Integrated Aircraft Development and Flight Testing'*, May 5-7, 1998, Madrid, Spain, paper 23

[3] V. BERTOGALLI, F. BISI, M. LOVERA: Modelling helicopter rotor dynamics with ADAMS, In *1995 ADAMS User Conference*, Ann Arbor, Michigan, USA, 1995

[4] *D. A. PETERS, N.* HAQUANG: Dynamic Inflow for Practical Applications*,* In *Journal of the American Helicopter Society,* Vol. 33, No. 4, October 1988, pp. 64-68

[5] J. ZHAO, J.V.R. PRASAD, D.A. PETERS: Dynamic Rotor Wake Distortion Model for Helicopter Maneuvering Flight, In *Proceedings of the 2002 Annual Forum of the American Helicopter Society*, Montreal, Canada, June 11-13, 2002.

[6] J. ZHAO, J.V.R. PRASAD, D.A. PETERS: Validation of a Rotor Dynamic Wake Distortion Model for Helicopter Maneuvering Flight Simulation, In *Proceedings of the 2004 Annual Forum of the American Helicopter Society*, Baltimore, Maryland, USA, June 7-10, 2004.

[7] W. JOHNSON: *Helicopter Theory*, Dover Publications Inc., New York, 1994

[8] R. PETTERSEN, E. MUSTAFIC, M. FOGH: *Nonlinear Control Approach to Helicopter Autonomy*, Master Thesis, Aalborg University, Denmark, 2005

[9] W. BITTNER: *Flugmechanik der Hubschrauber*, Springer, 3rd edition, Berlin, 2009

[10] R.E. SHELDAHL, P.C. KLIMAS: Aerodynamic characteristics of seven symmetrical airfoil sections through 180-degree angle of attack for use in aerodynamic analysis of vertical axis wind turbines, In *Technical Report SAND-80-2114*, Sandia National Labs., Albuquerque, New Mexico, USA, January 1981

[11] CYBERIAD: *Airfoil: NACA 0012 - Data: Lift Coefficients - Data: Drag Coefficients* www.cyberiad.net/library/airfoils/foildata/n0012cl.htm

[12] J.A. STALEY: Validation of Rotorcraft Flight Simulation Program through Correlation with Flight Data for Soft-in-Plane Hingeless Rotors, *Final Report*, U.S. Army Air Mobility Research and Development Laboratory, January 1976

[13] K.B. HILBERT: A mathematical model of the UH-60 helicopter, *NASA-TM-85890*, Defense Technical Information Center, 1984

[14] N.M. BEAULIEU: Validation of a Ground Dynamics Model Formulation By use of Landing Data, In *AIAA Modeling and Simulation Technologies Conference and Exhibit*, Paper AIAA 2006-6811, Keystone, Colorado, 21-24 August 2006

[15] E.N. JOHNSON AND P.A. DEBITETTO: Modeling and simulation for small autonomous helicopter development, In *AIAA Modeling and Simulation Technologies Conference*, New Orleans, Lousiana, 11-13 August 1997

[16] G.D. PADFIELD, A.T. MCCALLUM, H. HAVERDINGS, A. DEQUIN, D. HADDON, K. KAMPA, W. VON GRÜNHAGEN, P.M. BASSET: Predicting Rotorcraft Flying Qualities Through Simulation Modelling: A Review of Key Results from GARTEUR AG06. In *Proceedings of the 22nd European Rotorcraft Forum*, Brighton, UK, September 1996

[17] C.R. THEODORE: Helicopter Flight Dynamics Simulation with Refined Aerodynamic Modeling, *Dissertation*, University of Maryland, USA, 2000

[18] A. TEWARI: *Atmospheric and Space Flight Dynamics*, Birkhäuser, Boston, 2007